Atmos. Meas. Tech. Discuss., 5, 4249–4283, 2012
www.atmos-meas-tech-discuss.net/5/4249/2012/
doi:10.5194/amtd-5-4249-2012

Atmospheric Measurement Techniques Discussions

Observation of volcanic ash from Puyehue-Cordón Caulle with IASI

L. Klüser[1,2], **T. Erbertseder**[1], **and J. Meyer-Arnek**[1]

[1]Deutsches Zentrum für Luft- und Raumfahrt (DLR), Oberpfaffenhofen, Germany
[2]University of Augsburg, Institute for Physics, Augsburg, Germany

Received: 4 April 2012 – Accepted: 31 May 2012 – Published: 13 June 2012

Correspondence to: L. Klüser (lars.klueser@dlr.de)

Published by Copernicus Publications on behalf of the European Geosciences Union.

Abstract

On 4 June 2011 an eruption of the Chilean volcano complex Puyehue-Cordón Caulle injected large amounts of volcanic ash into the atmosphere and affected local life as well as hemisphere-wide air traffic. Observations of the Infrared Atmospheric Sounding Interferometer IASI flown on board of the MetOp satellite have been exploited to analyze the evolution of the ash plume around the Southern Hemisphere. A novel Singular Vector based retrieval methodology, originally developed for observation of desert dust over land and ocean, has been adapted to enable remote sensing of volcanic ash.

Since IASI observations in the 8–12 µm window are applied in the retrieval, the method is insensitive to solar illumination and therefore yields twice the observation rate of the ash plume evolution compared to solar backscatter methods from polar orbiting satellites. The retrieval scheme, the emission characteristics and the circumpolar transport of the ash are examined by means of a source-receptor analysis.

1 Introduction

Volcanic eruptions can emit large quantities of ash particles and gases, such as H_2O, CO_2 or SO_2 into the atmosphere. Depending on the injection height, volcanic ash can remain up to several weeks in the troposphere and up to months in the stratosphere. Following Halmer and Schmincke (2003) 80 % of ash emissions from explosive volcanic eruptions exceed altitudes of 6 km, 60 % of 10 km and 20 % altitudes of 15 km. Therefore, volcanic ash may also be subject of long range transport in the free troposphere and stratosphere.

In ambient air, volcanic ash poses a severe health risk to human beings and animals (Horwell and Baxter, 2006). Moreover volcanic ash has proven to be a hazard to aviation (Miller and Casadevall, 2000). Depending on concentration and composition it may strongly reduce visibility, clog the sensors of the aircraft, disturb the avionics and lead in the worst case to a failure of the turbojet engine (Swanson and Beget, 1991).

AMTD
5, 4249–4283, 2012

In the past more than 90 aircraft were damaged after flying through volcanic ash plumes. The total cost of the damage to aircraft in the period 1982–2000 is estimated at 250 million US dollar, but so far none of the incidents has resulted in fatal accidents (van Geffen et al., 2007). The eruption of the Icelandic volcano Eyjafjalla in May 2010 and the closure of the European air space has clearly demonstrated the vulnerability of the economy to such an "air disaster" (Zehner, 2010). Moreover it has demonstrated the importance of satellite data for tracking and early warning of volcanic emissions and, in particular, ash plumes.

So far, however, mainly observations of SO_2 and the ultraviolet aerosol absorbing index (Torres et al., 1998) have been used as a proxy for volcanic ash from satellite instruments like the Total Ozone Monitoring Spectrometer (TOMS), the Global Ozone Monitoring Experiment (GOME, GOME-2), Scanning Imaging Absorption Spectrometer for Atmospheric Cartography (SCIAMACHY) and the Ozone Monitoring Instrument (OMI) (e.g. Krueger et al., 1983; Thomas et al., 2005; Loyola et al., 2008; Rix et al., 2009; Krotkov et al., 2005).

Mineral aerosol extinction in the thermal infrared window is mainly caused by Si–O resonance absorption around 9.5 µm in silicates (e.g. Hudson et al., 2008a,b). Like desert dust, volcanic ash is largely composed of silicate materials (e.g. Pettijohn et al., 1972; Horwell and Baxter, 2006; Prata and Kerkmann, 2007). Prata (1989) showed that infrared split window satellite observations can be used to detect volcanic ash plumes. Different approaches of exploiting differential volcanic ash absorption in infrared satellite observations for ash detection have been applied to volcanic eruptions since (e.g. Wen and Rose, 1994; Hilger and Clarke, 2002; Prata and Bernado, 2009; Corradini et al., 2009; Karagulian et al., 2010). Recently, the Infrared Atmospheric Sounding Interferometer (IASI) on MetOp has been applied to detect volcanic SO_2 and to derive an ash index (Clarisse et al., 2008, 2010).

In this paper the adaptation to volcanic ash of a novel retrieval method for mineral dust is presented that enables remote sensing of volcanic ash aerosol optical depth (AOD) with IASI. The method is applied to a plinian eruption from a fissure

AMTD
5, 4249–4283, 2012

in the Puyehue-Cordón Caulle Volcanic Complex in central Chile which began on 4 June 2011 at 19:15 UTC (SERNAGEOMIN, 2011). Hereafter the eruption will be referred to as PCCE (Puyehue-Cordón Caulle eruption). It caused widespread ash fall and air space closure over South America, Australia and New Zealand. The ash plume could be detected south of Australia some days after the eruption and reached the Chilean coast from westerly directions again on 14 June 2011 after circumpolar transport.

After this introduction the ash retrieval method for IASI is described in Sect. 2, followed by observations and analysis of the PCCE ash plume. After a discussion in Sect. 4, conclusions are drawn in Sect. 5.

2 Volcanic ash retrieval from IASI

The Infrared Atmospheric Sounding Interferometer (IASI) is a Michelson interferometer developed for atmospheric sounding in the thermal infrared spectrum (Larar et al., 2010). It has a spectral resolution of 0.5 cm^{-1} (apodised) in 8641 channels at a ground resolution of 12 km (diameter) at nadir.

In Klüser et al. (2011) a methodology to retrieve mineral dust Aerosol Optical Depth (AOD) from observations from IASI was presented. This method uses Singular Vector Decomposition (SVD) for un-mixing the signals of (dust) aerosol, gas absorption and surface emissivity.

The approach extracts the aerosol information from the spectral extinction pattern matched to linear combinations of third and higher order singular vectors of IASI spectra.

The basic idea of the method is to apply a dust (or volcanic ash, as done here) observation method which does not rely on a priori assumptions such as atmospheric state or surface emissivity. Nevertheless one a priori assumption cannot be avoided – the use of spectral extinction properties of the observed aerosol (desert dust or volcanic ash). In Klüser et al. (2011) four different size distributions of mineral dust from the

AMTD
5, 4249–4283, 2012

Optical Properties of Aerosols and Clouds (OPAC) database (Hess et al., 1998) has been used, while in the recent version of the method extinction spectra of dust components measured by FTIR are used (Klüser et al., 2012; measurements of spectra described in Hudson et al., 2008a,b).

Instead of pre-calculating look-up table generated by radiative transfer modelling, dust- (or ash-) related "equivalent optical depth" spectra are calculated in the 8–12 µm (830–1250 cm^{-1}) window region (Klüser et al., 2011). For mathematical details of the retrieval algorithm the reader is kindly referred to Klüser et al. (2011) and only a short overview is presented here.

The IASI level 1C spectra of the window region (830–1250 cm^{-1}) are compiled into 42 bins with 10 cm^{-1} bin width (20 IASI channels each). The maximum brightness temperature of each bin is used as spectral information, thus minimising the absorption effect of narrow gas absorption lines. Then the "equivalent optical depth" τ_{eqv} is calculated from the observed radiance L_{obs} at wavenumber ν, the Planck-function B_ν of T_{base}, i.e. the maximum brightness temperature within the observation window ("baseline temperature") and the cosine of the viewing zenith angle (Θ_v):

$$L_{obs} = e^{\frac{\tau_{eqv}}{\cos\Theta_v}} B_\nu(T_{base}) \quad (1)$$

Singular vectors have been decomposed from equivalent optical depth spectra of seven days in March 2009 over the Sahara/Arabia domain and adjacent oceans. These singular vectors reflect the dominating modes of spectral variability in IASI spectra (given the assumption that volcanic ash has similar spectral extinction features as mineral dust – an assumption which is widely used in thermal infrared remote sensing, e.g. Volz, 1973; Corradini et al., 2009).

The leading two singular vectors account for most variability in the IASI spectra and can be attributed to surface emissivity and broad gas absorption (O_3, H_2O, CO_2). Consequently the dust respective ash signal is carried mainly by the higher order singular vectors (numbers three to six). For each singular vector the respective weight in a given observed spectrum is calculated as the scalar product of the singular vectors and the

AMTD
5, 4249–4283, 2012

τ_{eqv} spectrum (Eq. 1). The dust or ash related spectral signal is represented by the linear combination of the third and higher order singular vectors scaled by the respective weights. Projecting the normalised (to optical depth of 1 at 1000 cm^{-1}) dust/ash extinction spectrum onto the dust/ash related spectral extinction signal, i.e. the linear combination of weighted higher order singular vectors, provides an estimate of the infrared optical depth of dust/ash at 1000 cm^{-1} represented by the respective dust/ash component. This is done for each dust/ash component separately. By the projection method also the weighting of the different components can be obtained as the "angle" between the theoretical AOD spectrum and the singular vector linear combination (see Klüser et al., 2011 for mathematical details). From the weights of the different components the assumed dust/ash extinction spectrum is calculated as a simple linear combination of weighted extinction spectra of the components and another initial estimate of dust/ash AOD at 1000 cm^{-1} is obtained by the projection approach. From this AOD estimate the effective dust emission temperature can be estimated. The observed radiance spectra are then corrected for the contribution of dust emission and a second iteration of the retrieval yields then dust/ash infrared AOD.

Also the leading two singular vectors carry some information on the dust/ash extinction. This information is accounted for by an additive correlation correction of the infrared AOD.

The SVD technique is applied to τ_{eqv} rather than radiance or brightness temperature. Moreover broadband gas absorption is contained in the leading two singular vectors. Consequently the higher order singular vectors are mainly sensitive to dust/ash absorption features. The height of dust/ash layers affects radiance spectra in two ways: thermal emission by the aerosol itself (which is accounted for in the iterative retrieval process) and the signal attenuation due to molecular absorption in the atmosphere. The latter is reflected in lower atmospheric density and thus opacity for higher dust/ash layers and varies spectrally. This signal is mainly contained in the leading two singular vectors. Using an additive correlation correction for the signal contained in the leading two singular vectors (partly) accounts for the effect of dust/ash layer height: the

AMTD
5, 4249–4283, 2012

correction can be positive in cases of underestimation of AOD due to high gas opacity (relevant for low level aerosol) or negative in cases of overestimation of AOD due to surface emissivity and low gas opacity (relevant for elevated aerosol layers), depending on the observed spectra.

The validation of IASI derived dust AOD could be largely improved by including variable mineralogy and accounting for non-sphericity of the particles compared to using OPAC spectra (Klüser et al., 2012). One of the major advantages of the Singular Vector based un-mixing approach is that dust (and as will be shown in this paper volcanic ash) can also be observed above land, where surface emissivity is unknown. Moreover silicate aerosols can also be detected above underlying clouds.

Extinction spectra of dust and volcanic ash in the 8–12 µm range have large similarity, as both are mainly composed of silicate materials (e.g. Volz, 1973). Nevertheless mineralogy and particle sizes of volcanic ash may strongly differ from dust assumptions (Volz, 1973), especially regarding the apparent absence of clays and the higher feldspar abundance as well as the presence of mafic minerals (Pettijohn et al., 1972). Hudson et al. (2008a,b) presented a method to better represent non-sphericity in extinction modeling. As for non-clayey desert dust components (Klüser et al., 2012) the "continuous distribution of ellipsoids" (CDE) approach has been used in this study for modeling of the extinction cross section $C_{\mathrm{CDE}}(v)$ of volcanic ash components:

$$C_{\mathrm{CDE}}(v) = kv \cdot \mathrm{Im}\left[\frac{2\varepsilon}{\varepsilon - 1}\log(\varepsilon)\right] \tag{2}$$

$\varepsilon = \varepsilon' + i\varepsilon''$ is the complex dielectric constant (the property provided by the references for optical constants, Table 1), the size parameter k is calculated as $2\pi/\lambda$ with wavelength λ, and v is the particle volume. It is related to the diameter D of a spherical particle of equivalent volume by $v = \pi D^3/6$ (see e.g. Hudson et al., 2008a,b). From the modeled spectral extinction cross sections of the ash components the extinction spectra used in the retrieval are easily obtained by normalization to AOD = 1 at 1000 cm^{-1}. This approach assumes that the spectral extinction is generally represented by absorption

AMTD
5, 4249–4283, 2012

and that scattering can be neglected (see Hudson et al., 2008a,b). Consequently the retrieved infrared optical depth of the dust/ash is absorption optical depth.

The eight mineral components used for ash retrieval together with their source of optical constants are presented in Table 1, while the resulting extinction spectra are depicted in Fig. 1. The spectra are normalized by the integrated extinction over the retrieval domain (833 cm^{-1}–1250 cm^{-1}, equals 8 µm–12 µm in wavelength space) in Fig. 1 for visualisation purpose.

The list of components is definitely not complete to consider all volcanic minerals. However, eight components are sufficient for the retrieval of volcanic ash in reasonable computing time. They also provide enough spectral variability to search for the best fit in the observations. Moreover these spectra represent a selection of minerals with rather strong deviations in spectral features between each other compared to other minerals. Therefore it is not envisaged or suggested that the retrieval components cover the full mineralogy of volcanic ash. Although the mineral extinction models are selected to fit volcanic ash plumes, they also have to include silicates which are also abundant in desert dust (e.g. SiO_2, feldspars). Thus the retrieval will also be sensitive to airborne mineral dust.

As described in Klüser et al. (2012) the effective size of the ash particles is estimated directly from the modeled extinction (and thus not independently from optical depth), which is itself a direct function of particle volume (Hudson et al., 2008 a,b). Together with (size dependent) extinction efficiency Q_{ext} (e.g. Wen and Rose, 1994) the effective particle diameter D_{eff} can be used to derive aerosol mass (e.g. Wen ad Rose, 1994; Prata and Kerkmann, 2007; Corradini et al., 2009; Prata and Bernado, 2009):

$$\frac{M}{A} = \frac{2\pi\rho_{ash} D_{eff} \mathrm{AOD}_{10\,\mu m}}{3Q_{ext}(D_{eff}, 10\,\mu m)} \tag{3}$$

with unit area A and ash particle density ρ_{ash}. In the method homogeneity of the ash layer over the IASI footprint is assumed (as also e.g. AOD is a quantity integrated over the footprint). The ash particle density is calculated from tabulated mean densities

AMTD
5, 4249–4283, 2012

of mineralogical components weighted as retrieved by the algorithm. One should be aware that the retrieval is mainly sensitive to silicates by nature. Thus ash mass might be underestimated due to undetected non-silicate components of the ash plume. Moreover ice coated ash particles are not detected as they appear as ice clouds in the retrievals. Wen and Rose (1994) estimate from sensitivity analysis that such mass retrievals may have errors of about 40–50 %. As the effective particle size is not retrieved independently (Klüser et al., 2012) and consequently is closely linked to the optical depth retrieval, the use of retrieved effective radius introduces another error source which, together with the intrinsic retrieval uncertainty (Klüser et al., 2011) adds to the uncertainty estimate of Wen and Rose (1994) in the presented method.

Ice clouds can also be detected from IASI with the same method as the ash retrieval run with ice cloud optical properties (Warren, 1984). Retrieved ice cloud information is used qualitatively only due to lacking validation and the limitation of quantitative information to moderately thick ice clouds (Comstock et al., 2010).

3 Observation and analysis of the ash plume

Figure 2 shows the evolution of the PCCE ash plume during the initial phase of the eruption as seen in IASI AOD. The volcano is indicated in the maps by the black triangle near the plume origin in Chile. The plume evolution is depicted for each overpass of the MetOp satellite, i.e. at about 09:45 LT in the morning (descending orbits) and about 21:45 LT in the evening (ascending orbits). The retrieval has been limited to latitudes between 20° S and 60° S in order to reduce processing costs. Ash optical depth at 10 µm reaches values of more than 1.5 in the plume center. The plume is covered very well by the IASI observations, although there are hardly any observations directly above the volcano. It is obvious that some lower mineral AOD observations over northern parts of Chile are not related to the PCCE plume (especially on 6 June). These may well be observations of airborne desert dust.

AMTD
5, 4249–4283, 2012

Figure 3 shows the volcanic ash plume through the subsequent days (7 and 8 June). On 7 June parts of the plume directly above the volcanic source and also North of 30° S are missed due to orbit gaps and ice clouds (see Fig. 4). The missed ash is advected further east and again detected at the Atlantic Ocean coast in the evening (visible on 8 June in Fig. 3). Pettijohn et al. (1972) report differences in sands of volcanic and aeolian origin being represented by different quartz to feldspar ratios and the abundance of pyroxenes and olivines in volcanic materials. If the mineralogical information of the retrieval can be used for separating between pyroclastic and terrigenous aerosols and if the mineralogical components have to be updated for this purpose will be the subject of further research in the future.

It is not possible with IASI to retrieve volcanic ash AOD below or within ice clouds. Moreover within the 12 km IASI pixels mixtures of ice and ash or ice coatings on ash particles may occur. Thus one is also interested in the position and opacity of ice clouds. As a first assessment resulting extinction spectra of the ash plume are mixed with ice cloud extinction spectra (Warren, 1984) for ice cloud contributions of 0 %, 25 %, 50 %, 75 % and pure ice cloud. For each ash-ice mixture the correlation coefficient between composed ash-ice extinction spectrum and observed linear combination of weighted singular vectors is calculated and the respective ice abundance is weighted with the normalized correlation, yielding the ice cloud probability for the respective pixel. Ice cloud probabilities within ash observations (with $AOD_{10\,\mu m} > 0.1$ only) are depicted in the top row of Fig. 4 for 7 and 8 June descending orbits. Moreover the ice cloud extinction spectra can be used to calculate an ice cloud index by correlating them to the IASI spectra (bottom row of Fig. 4). Index values above 50 (correlation times 100) indicate opaque ice clouds while lower values indicate potential thin ice cloud contamination of the observations. It is evident from Fig. 4 that in cases the ash plume is transported very close to and potentially partly within or beneath ice clouds.

Given the assumption that the ash mass as retrieved by Eq. (1) is representative for the ash mass column (with large error bars, intrinsic retrieval uncertainty), the total airborne ash mass can be estimated by integration over all IASI observations showing

AMTD
5, 4249–4283, 2012

volcanic ash. The respective time series, separated by ascending and descending orbits, is presented in Fig. 5.

In order to examine the retrieval scheme for the PCCE event, the sensitivity of IASI aerosol optical depth thresholds and the maximum retrieval uncertainty is investigated. For the analysis the threshold values for aerosol optical depth are varied between 0.1 and 0.3 and the intrinsic retrieval uncertainty between threshold values ranging from 30 % to 50 %. The results of the evaluation are summarized in Table 2. Selecting conservative criteria with retrieval uncertainties less than 30 % and aerosol optical depths thresholds larger than 0.2, results in 1874 IASI observations for the PCCE event from 5 to 14 June. By applying these conservative criteria the noise level of the observational data can be reduced to a minimum. When selecting an even stricter threshold for aerosol optical depth of larger than 0.3 (and uncertainty less than 30 %), no ash observations remain for 11 June and 14 June.

All IASI observations are assigned to specific sources i.e. the PCCE or mineral dust by a simple source-receptor analysis using the backward trajectory matching technique (Thomas et al., 2005). Following the sensitivity analysis above, all IASI ash observations with an aerosol optical depth larger than 0.2 and a retrieval uncertainty less than 30 % from 5 June to 14 June are examined (1874 observations). Ensembles of backward trajectories are calculated using the three-dimensional kinematic trajectory model FLEXTRA (Stohl et al., 1999) which is driven by wind fields from the Global Forecasting System (GFS) of the National Center for Environmental Prediction (NCEP) with a 6 h resolution interpolated to 3 h. The trajectories are released using the spatial and temporal characterization of the IASI observations as starting conditions and integrated backwards for 240 h. Since the height of the ash plume in the (vertically integrated) observations remains unknown, the trajectories are initialized every 250 m from 1 km to 15 km altitude. Filtering the resulting ensemble of trajectories for the PCCE source allows confirming the volcanic origin of the detected (ash) particles and excluding other sources. It enables to estimate the effective emission height over the volcano as well as the effective height of the ash plume using the vertical wind shear. The accuracy of

AMTD
5, 4249–4283, 2012

the trajectory matching approach was evaluated in Thomas et al. (2005) using ground-based measurements of SO_2 and aerosols.

Figure 6 shows the backward trajectories released for all IASI observations as described above on 11 June and 13 June, filtered for PCCE. Please note that the highest trajectories are plotted on top. Despite a transport time of up to over 192 h, ash observations can be assigned to the PCCE. The altitude range of the trajectories that can be traced back to an emission on 4 June and 5 June, varies from 6 to 16 km. The effective emission height for the initial eruption based on these selected observation dates can be assigned to 9 to 16 km. Using the observations on 13 June, For the subsequent eruption on 11 June altitude levels of the plume between 4 and 7 km are exhibited, while the effective emission height can be confined from 5 to 7 km . The ash observations at 45° W/40° S on 13 June originate from a repeat minor eruption on 12 June and can be assigned to altitude levels between 9 and 11 km.

Coherent long-range transport of the ash plume can be seen for the whole period. The source-receptor analysis for 11 June still represents well the pronounced wind shear to the east of Chile that could be observed by IASI (see Fig. 2). Ensembles of trajectories stay coherent depending on the effective emission height.

Evaluating the results of the trajectory analysis described above, Fig. 7 shows the percentage of IASI observations per day that can be assigned to the PCCE source. The given dates refer to the date of observation. Despite the application of a simple source-receptor analysis and global wind fields it can be demonstrated that the majority of observations from 5 June to 12 June can be assigned to the PCCE. It is also evident that the numbers decrease with increasing travel time up to 216 h taking into account that the majority of ash was released on 5 to 6 June. However, the result is somewhat disturbed as such that continued ash emissions prevail till 13 June.

By means of analyzing all IASI observations between 5 June and 14 June with the backward trajectory matching technique described above, the effective emission height for the PCCE is estimated. All trajectories arriving over the volcano in a 1° × 1° grid

AMTD
5, 4249–4283, 2012

box centered at the source are filtered and normalized trajectory densities derived as a function of time and altitude.

The estimated effective emission height for the volcanic ash at PCC is depicted in Fig. 8 and follows well the independent observations mainly from ground reported by SERNAGEOMIN (2011): the onset of the PCCE on 4 June, 19:15 UTC is captured (within the given temporal uncertainty of the wind fields: 6 h interpolated to 3 h resolution according to Stohl et al., 1999). On 4 June and 5 June the lower part ranging from 3 to 7 km (that was transported to the southeast) is well separated from an upper part above 9 km (that was transported to the east) (see Fig. 2). On 5 June an ash layer was observed by aircraft pilots at flight level 390/400 which corresponds to an altitude of approximately 12 km. This can be recognized well in the Fig. 8 as maximum densities (given the uncertainties of the approach in particular to limitations in the vertical resolution). This is confirmed by local observatories which report an eruptive column of about 10 to 12 km height for 5 June. According to the reports from ground the eruptive column lowers down to 10 km on 6 June (13:00 UTC). The subsequent eruptive phases on 7 June, 8 June, 11 June, and 13 June are also reproduced in the normalized trajectory densities above the volcano. The height regimes for the analyzed period are captured well starting with an eruptive column exceeding 10 km but remaining below that level for the subsequent eruptions (when considering the maxima of the trajectory densities at the source). The maximum heights of the eruptive columns of the subsequent eruptions were estimated from ground to 7.5 km on 8 June, 4 and 8 km on 11 June and 8 km on 13 June. The weak vertical structure of the analysis on 11 and 13 June indicates that some uncertainty is introduced by a missing or weak wind shear and in addition short travel times of the trajectories.

Derived emissions before the actual onset of the eruption clearly reflect further uncertainty introduced by the coarse resolution wind fields and thus the overall limitation and dependency on the quality of the wind fields.

In the following the results for the forward simulation with the Lagrangian Particle Dispersion Model FLEXPART (Stohl et al., 2005) are presented. For this study no

AMTD
5, 4249–4283, 2012

a priori information is used. Particles with a unit mass were emitted above Puyehue-CordónCaulle from 2 to 14 km above ground in height level slices of 1000 m. They are continuously released at a frequency of 6 h from 4 June to 13 June. Such an approach has been introduced to study SO_2 emission profiles of the Jebel at Tair eruption in 2007 (Eckhardt et al., 2008).

The FLEXPART particle dispersion model computes trajectories of air tracer parcels being advected by the wind. Moreover, sub-scale processes introducing increased dispersion as well as particle removal due to chemical reactions are considered. In our study, the particles are regarded as passive tracers, hence no chemical conversion takes place.

The dispersion model simulation is driven by the identical GFS forecasts which have been applied by the trajectory analysis (already discussed above).

To derive the PCCE source vertical emission profile, all emitted particles are followed and continuously compared to IASI ash observations. Both, the modeled particles and the IASI observations are binned into a $0.5^\circ \times 0.5^\circ$-grid. In the case that IASI observations coincide with modeled particles in space and time, the release time and altitude of this model run is tagged with a certain score. The score depends linearly on the travel time of the air parcel and on the amount of binned pixels overlapping.

This implies that the score increases the longer the emission is dated back and the better the overlap of the modeled particles with IASI observations is. Finally the score is normalized for the three consecutive emission episodes of the PCCE individually, resulting in a quantity referred to as normalized particle density profile (see Fig. 9).

For the whole episode, 1354 coincidences of modeled and observed particle bins are diagnosed. 38 bins of IASI ash observations can not be matched modeled particles. Most of them are likely due to observations of desert dust.

Although the inversion by particle dispersion modeling is initialized at a much coarser vertical and temporal discretization the key patterns in the effective emission profiles remain (when comparing Figs. 8 and 9). However, some deviations are obvious like lower maximum emission heights in the initial eruption phase on 5 June and on 11 June.

AMTD
5, 4249–4283, 2012

4 Discussion

The IASI method is able to observe the evolution of the PCCE ash plume on a full cycle around the Southern Hemisphere. In contrast to methods using backscattered solar radiation, thermal infrared methods like the presented one for IASI are capable to observe the ash plume regardless of solar illumination. Consequently the sampling rate can be doubled from polar orbiting platforms like MetOp.

In the set up used for volcanic ash retrieval the method has not yet been validated, thus the results rather show the potential of the method then quantitatively accurate results. Nevertheless in Klüser et al. (2012) it has been shown that the improvement of the method with respect to variable mineralogy is capable of quantitative dust monitoring and validation results could be largely improved. Also a widely used method of converting ash optical depth and particle size into ash mass column has been applied and results have also been presented by means of ash mass, being very aware that presentation of ash mass is connected to very large uncertainties. Two major uncertainties of qualitative ash monitoring with IASI still remain. It is not and probably will never be possible from satellite to assess the ash particles masked by overlying cirrus or coated with ice crystals. Nevertheless IASI offers the possibility to obtain also valuable information on ice clouds and a rough indication of ice abundance within ash plume observations. It could be confirmed that ice coating and masking by ice clouds are both relevant for monitoring of long range transport of volcanic ash. Moreover distinguishing volcanic ash from other aerosols remains an unsolved problem, especially for monitoring and alerting purposes. The IASI method has been shown to be sensitive to coarse mode, mainly silicate, aerosol particles only in the desert dust set-up (Klüser et al., 2012). Thus it can be assumed on a sound basis that also the volcanic ash set-up is insensitive to other aerosol types such as industrial aerosols, biomass burning aerosol or sea salt, especially as in the volcanic ash version only silicate spectra are exploited for retrieval. Nevertheless it is not yet clear if separation between volcanic ash and desert dust will become possible from the contained mineralogical information. The

AMTD
5, 4249–4283, 2012

assessment of the information content regarding mineralogy and consequently methods to flag the observations as either volcaniclastic or terrigenous, e.g. by quartz to feldspar ratios or pyroxene abundance (Pettijohn et al., 1972), will be the subject of research in the near future. Evaluated mineralogical constrains will furthermore reduce uncertainties of the mass retrieval as mineral densities vary to a much higher degrees in pyroclastic than in terrigenous minerals.

The current set up of the volcanic ash retrieval uses modeled extinction spectra. Hudson et al. (2008a,b) clearly showed that modeling extinction spectra, also with methods better suited than Mie theory, does not fully represent spectral variability of mineral extinction. Thus the modeled extinction spectra have to be regarded as another source of uncertainty – especially also when transfer to visible wavelength AOD is envisaged. Due to the often much higher iron content in pyroclastic materials compared to desert dust absorption at solar wavelengths in volcanic ash plumes cannot be assumed to be represented by any approximation inferred from desert dust. Also the transfer of infrared optical depth to visible wavelengths will be looked into in more detail in the future.

By means of ensemble backward trajectory matching and forward Lagrangian particle dispersion modeling without using a priori information the source-receptor relationship could be analyzed and the volcanic origin of the majority of the IASI observations proven. In doing so the effective emission height of the ash at PCC has been estimated and an indication of the plume height could be derived. Therefore these approaches add information content to the vertically integrated IASI ash observations which is very relevant for aviation safety and studies of stratospheric injections. A comparison with observations mainly from ground shows good agreement, given the use of global wind field at 6 h resolution.

Despite the existence of more sophisticated inversion schemes as applied in Stohl et al. (2011) for the eruption of Eyjafjalla in Iceland these simple approaches have proven to be robust and efficient for the purpose of analyzing a qualitative source-receptor relationship in a near-real-time environment. Ensemble backward trajectory

AMTD
5, 4249–4283, 2012

matching and forward Lagrangian particle dispersion modeling methods are simple compared to a full inversion of the Lagrangian transport (Seibert et al., 2011) or adjoint retroplume approaches (Issartel and Baverel, 2003), but are still among the suite of applied methods (Baklanov et al., 2011).

However, all methods strongly rely on the vertical wind shear and depend on the quality of the wind fields. In this study global wind fields from the Global Forecasting System (NCEP) at 6 h resolution interpolated to 3 h have been used. Kristiansen et al. (2011) have compared these wind fields to alternative data from the European Center for Medium Range Weather Forecast (ECMWF) and found that the source terms were robust to which meteorological data was used. Still the global data sets exhibit a coarse resolution compared to the pronounced orography in the Andes and the volcanic fissure of PCC in particular. Furthermore, micro- and meso-scale processes triggered by the eruption significantly influence the local meteorology. Seibert et al. (2011) conclude, however, that eruption column models are not a good alternative. Especially in near-real time and for volcanoes that are not monitored well, detailed knowledge of eruption source parameters is lacking. Since the focus in this study is on examining the hemispheric transport local effects at the volcano are not considered and global wind fields justified. As can be inferred from Figs. 8 and 9, however, the derived emission profiles prior to the actual onset of the eruption clearly reflect the uncertainty introduced by the coarse resolution wind fields and thus the overall limitation of the inversion methods.

5 Conclusions

A method previously developed for desert dust remote sensing with IASI has been adapted for retrieving infrared optical depth and mass of volcanic ash plumes. The application of thermal infrared observations without a priori assumptions enables to observe ash plumes twice daily over land, over ocean and also above low-level clouds. The volcanic ash retrieval method uses extinction spectra of different mineral

AMTD
5, 4249–4283, 2012

components found in volcanic ash rather than fixed ash refractive indices. As spherical Mie calculations cause significant errors in positions and strengths of Si-O resonance peaks the extinction spectra are modeled with non-spherical approximations. The different mineralogical components are weighted by a Singular Vector based projection scheme also accounting for surface emissivity effects in the observed radiance. Validation efforts for desert dust retrievals showed a large positive impact of the application of variable mineralogy compared to fixed optical properties. It can be assumed that also the volcanic ash retrieval benefits from the accounting for variable mineralogy of the plume. If the weights of the respective mineral components relate to the true mineralogy of the plume and thus can be used for distinguishing between pyroclastic and terrigenous plumes cannot yet be concluded, although initial tests indicated that at least some information is contained in the retrieval results. It will be investigated in the future if such information can be derived reliably and consequently if the retrieval of ash mass can benefit from the characterization of the mineralogical composition of the plume. Furthermore it has to be investigated in detail, if visible optical depth can be derived reliably, which is largely controlled by particle size and iron content besides infrared optical depth.

By applying the novel IASI retrieval scheme the plume of the 2011 Puyehue-Cordón Caulle eruption (PCCE) could be tracked along its circum-polar transport in the Southern Hemisphere from 5 June to 14 June. On 14 June parts of the ash emitted by PCCE arrived again at the source region from westerly directions. The IASI observations have been examined by means of ensembles of backward trajectories and forward particle dispersion modeling without using a priori information. In doing so, the source-receptor relationship could be analyzed and the volcanic origin of the majority of the IASI observations proven. In addition the effective emission height of the ash at the volcano through the different eruption phases has been estimated and an indication of the plume height could be derived. A comparison with observations mainly from ground, as reported by SERNAGEOMIN (2011), shows fairly good agreement, given the use of global winds fields at 6 h resolution and the dependency on vertical wind shear. While

AMTD
5, 4249–4283, 2012

the ash was repeatedly emitted into the troposphere at height levels between 3 km and 9 km, during the peak of the eruption on 5 June the ash was possibly emitted up to 15 km. Both methods clearly indicate an emission peak between 9 km and 14 km. Observations from aircraft report ash at flight levels around 12 km. Although two simple modeling approaches were applied, information content is added to the vertically integrated IASI ash observations, which is very relevant for aviation safety and studies of stratospheric injections.

The focus of the source-receptor analyses performed here has been to examine the IASI retrievals qualitatively with respect to distinguishing between mineral dust and volcanic ash. Supplementary the potential of retrieving additional characteristics of the eruption like effective emission height and plume height has been demonstrated without addressing ash concentrations. More quantitative approaches will be applied in a follow up study, when the IASI ash retrievals will be evaluated in more detail using independent observations when they become available.

The direct retrieval of the plume height is possible from infrared methods at least over ocean (Pierangelo et al., 2004). A similar approach of plume height retrieval will be added to the current method in the future. Comparing retrieved plume heights with ensemble backward-trajectory or particle dispersion modeling inferred plume height distributions will give additional uncertainty information to the plume height. Reliable mass (to be obtained from AOD and effective particle size) and plume height information may then be used for assimilation in numerical ash prediction models. In general, more quantitative methods to better consider and evaluate ash concentrations and their uncertainty are needed. A close collaboration between remote sensing and atmospheric modelling is essential to further characterize and elaborate the uncertainties in both, observations and analysis, and to improve the derivation of the source function for volcanic ash. It is expected that the presented ash retrieval from IASI in combination with inversion modeling and data assimilation will significantly improve the reliability of ash plume forecasts for aviation safety.

AMTD
5, 4249–4283, 2012

Acknowledgements. We are thankful to EUMETSAT and the EUMETSAT Data Centre (UMARF) for providing the IASI observations from METOP. We kindly acknowledge Andreas Stohl and all contributing colleagues for providing the models FLEXTRA and FLEXPART. Further thanks to the National Center for Environmental Prediction (NCEP) for making available the meteorological data of the Global Forecasting System (GFS).

References

Aronson, J. R.: Optical constants of monoclinic anisotropic crystals: orthoclase, Spectrochim. Acta, 42A, 187–190, 1986.

Aronson, J. R., Emslie, A. G., Smith, E. M., and Strong, P. F.: Infrared spectra of lunar soils and related optical constants, P. Lunar Planet. Sci. C., 10, 1787–1795, 1979.

Baklanov, A., Aloyan, A., Mahura, A., Arutyunyan, V., and Luzan, P.: Evaluation of source receptor relationship for atmospheric pollutants using approaches of trajectory modelling, cluster, probability fields analyses and adjoint equations, Atmospheric Pollution Research, 2, 400–408, doi:10.5094/APR.2011.045, 2011.

Clarisse, L., Coheur, P. F., Prata, A. J., Hurtmans, D., Razavi, A., Phulpin, T., Hadji-Lazaro, J., and Clerbaux, C.: Tracking and quantifying volcanic SO_2 with IASI, the September 2007 eruption at Jebel at Tair, Atmos. Chem. Phys., 8, 7723–7734, doi:10.5194/acp-8-7723-2008, 2008.

Clarisse, L., Prata, F., Lacour, J.-L., Hurtmans, D., Clerbaux, C., and Coheur, P.-F.: A correlation method for volcanic ash detection using hyperspectral infrared methods, Geophys. Res. Lett., 37, L19806, doi:10.1029/2010GL044828, 2010.

Comstock, J. M., d'Entremont, R., DeSlover, D., Mace, G. G., Matsorov, S. Y., McFarlane, S. A., Minnis, P., Mitchell, D., Sassen, K., Shupe, M. D., Turner, D. D., and Wang, Z.: An intercomparison of microphysical retrieval algorithms for upper-tropospheric ice clouds, B. Am. Meteorol. Soc., 88,191–204, 2007.

Corradini, S., Merucci, L., and Prata, A. J.: Retrieval of SO_2 from thermal infrared satellite measurements: correction procedures for the effects of volcanic ash, Atmos. Meas. Tech., 2, 177–191, doi:10.5194/amt-2-177-2009, 2009.

Eckhardt, S., Prata, A. J., Seibert, P., Stebel, K., and Stohl, A.: Estimation of the vertical profile of sulfur dioxide injection into the atmosphere by a volcanic eruption using satellite col-

AMTD
5, 4249–4283, 2012

umn measurements and inverse transport modeling, Atmos. Chem. Phys., 8, 3881–3897, doi:10.5194/acp-8-3881-2008, 2008.
Halmer, M. M. and Schmincke, H.-U.: The impact of moderate-scale explosive eruptions on stratospheric gas injections, B. Volcanol., 65, 433–440, 2003.
Hess, M., Koepke, P., and Schult, I.: Optical properties of aerosols and clouds: the software package OPAC, B. Am. Meteorol. Soc., 79, 831–844, 1998.
Hilger, D. W. and Clarke, J. D.: Prinicipal component analysis of MODIS for volcanic ash part most important bands and implications for future GOES campaigns, J. Appl. Meteorol., 41, 985–1001, 2002.
Horwell, C. J. and Baxter, P. J.: The respiratory health hazards of volcanic ash: a review for volcanic risk mitigation, B. Volcanol., 69, 1–24, 2006.
Hudson, P. K., Young, M. A., Kleiber, P. D., and Grassian, V. H.: Coupled infrared extinction spectra and size distribution measurements for several non-clay components of mineral dust aerosol (quartz, calcite and dolomite), Atmos. Environ., 42, 5991–5999, 2008a.
Hudson, P. K., Gibson, E. R., Young, M. A., Kleiber, P. D., and Grassian, V. H.: Coupled infrared extinction and size distribution measurements for several clay components of mineral dust aerosol, J. Geophys. Res., 113, D01201, doi:10.1029/2007JD008791, 2008b.
Issartel, J.-P. and Baverel, J.: Inverse transport for the verification of the Comprehensive Nuclear Test Ban Treaty, Atmos. Chem. Phys., 3, 475–486, doi:10.5194/acp-3-475-2003, 2003.
Karagulian, F., Clarisse, L., Clerbaux, C., Prata, A. J., Hurtmans, D., and Coheur, P. F.: Detection of volcanic SO_2, ash and H_2SO_4 using the Infrared Atmospheric Sounding Interferometer (IASI), J. Geophys. Res., 115, D00L02, doi:10.1029/2009JD012786, 2010.
Klüser, L., Martynenko, D., and Holzer-Popp, T.: Thermal infrared remote sensing of mineral dust over land and ocean: a spectral SVD based retrieval approach for IASI, Atmos. Meas. Tech., 4, 757–773, doi:10.5194/amt-4-757-2011, 2011.
Klüser, L., Kleiber, P., Holzer-Popp, T., and Grassian, V. H.: Desert dust observation from space – application of measured mineral component infrared extinction spectra, Atmos. Environ., 54, 419–427, doi:10.1016/j.atmosenv.2012.02.011, 2012.
Koike, C., Hasegawa, H., Asada, N., and Komatuzaki, T.: Optical constants of fine particles for the infrared region, Mon. Not. R. Astron. Soc., 239, 127–137, 1989.
Kristiansen, N. I., Stohl, A., Prata, A. J., Bukowiecki, N., Dacre, H., Eckhardt, S., Henne, S., Hort, M. C., Johnson, B. T., Marenco, F., Neininger, B., Reitebuch, O., Seibert, P., Thomson, D. J., Webster, H. N., and Weinzierl, B.: Performance assessment of a volcanic ash

AMTD
5, 4249–4283, 2012

transport model mini-ensemble used for inverse modeling of the 2010 Eyjafjallajökull eruption, J. Geophys. Res., 117, D00U11, doi:10.1029/2011JD016844, 2012.
Krotkov, N. A., Carn, S. A., Krueger, A. J., Bhartia, P. K., and Yang, K.: Band Residual Difference algorithm for retrieval of SO_2 from the Aura Ozone Monitoring Instrument (OMI). IEEE T. Geosci. Remote, 44, 1259–1266, doi:10.1109/TGRS.2005.861932, 2006.
Krueger, A. J.: Sighting of El Chichon sulfur dioxide clouds with the Nimbus 7 total ozone mapping spectrometer, Science, 220, 1377–1379, 1983.
Larar, A. M., Smith, W. L., Zhou, D. K., Liu, X., Revercomb, H., Taylor, J. P., Newman, S. M., and Schlüssel, P.: IASI spectral radiance validation inter-comparisons: case study assessment from the JAIVEx field campaign, Atmos. Chem. Phys., 10, 411–430, doi:10.5194/acp-10-411-2010, 2010.
Loyola, D., van Geffen, J., Valks, P., Erbertseder, T., Van Roozendael, M., Thomas, W., Zimmer, W., and Wißkirchen, K.: Satellite-based detection of volcanic sulphur dioxide from recent eruptions in Central and South America, Adv. Geosci., 14, 35–40, doi:10.5194/adgeo-14-35-2008, 2008.
Miller, T. P. und T. Casadevall. Volcanic ash hazards to aviation, in: Encyclopedia of Volcanoes, edited by: Sigurdsson, H., Academic Press, San Diego, California, USA, 2000.
Pettijohn, F. J., Potter, P. E., and Siever, R.: Sand and Sandstone, Springer Verlag, New York, USA, 1972.
Pierangelo, C., Chédin, A., Heilliette, S., Jacquinet-Husson, N., and Armante, R.: Dust altitude and infrared optical depth from AIRS, Atmos. Chem. Phys., 4, 1813–1822, doi:10.5194/acp-4-1813-2004, 2004.
Prata, A. J.: Observations of volcanic ash clouds in the 10–12 µm window using AVHRR/2 data, Int. J. Remote Sens., 10, 751–761, 1989.
Prata, A. J. and Bernardo, C.: Retrieval of volcanic ash particle size, mass and optical depth from a ground-based thermal infrared camera, J. Volcanol. Geoth. Res., 186, 91–107, 2009.
Prata, A. J. and Kerkmann, J.: Simultaneous retrieval of volcanic ash and SO_2 using MSG-SEVIRI measurements, Geophys. Res. Lett., 34, L05813, doi:10.1029/2006GL028691, 2007.
Rix, M., Valks, P., Hao, N., van Geffen, J., Clerbaux, C., Clarisse, L., Coheur, P.-F., Loyola, D., Erbertseder, T., Zimmer, W., and Emmadi, S.: Satellite monitoring of volcanic sulfur dioxide emissions for early warning of volcanic hazards, IEEE J. Sel. Top. Appl., 2, 196–206, 2009.

AMTD
5, 4249–4283, 2012

Roush, T., Pollack, J., and Orenberg, J.: Derivation of Midinfrared (5–25 µm) optical constants of some silicates and palagonite, Icarus, 94, 191–208, 1991.
Seibert, P., Kristiansen, N. I., Richter, A., Eckhardt, S., Prata, A. J., and Stohl, A.: Uncertainties in the inverse modelling of sulphur dioxide eruption profiles, Geomatics, Natural Hazards and Risk, 2, 201–216, 2011.
SERNAGEOMIN (Servicio Nacional de Geologia y Mineria): Reportes Escpeciales de Actividad Volcanica No 27–39, Observatorio Volcanologico des los Andes del Sur (OVDAS), Red Nacional de Vigilancia Volcanica (RNVV), retrieved from http://www2.sernageomin.cl/ovdas/ovdas7/informativos2/informes_ovdas01.php (last access: June 2012), 2011.
Servoin, J. L. and Piriou, B.: Infrared reflectivity and raman scattering of Mg_2SiO_4 single crystal, Phys. Status Solidi B, 55, 677–686, 1973.
Stohl, A., Haimberger, L., Scheele, M., and Wernli, H.: An intercomparison of results from three trajectory models, Meteorol. Appl., 8, 127–135, 1999.
Stohl, A., Forster, C., Frank, A., Seibert, P., and Wotawa, G.: Technical note: The Lagrangian particle dispersion model FLEXPART version 6.2, Atmos. Chem. Phys., 5, 2461–2474, doi:10.5194/acp-5-2461-2005, 2005.
Stohl, A., Prata, A. J., Eckhardt, S., Clarisse, L., Durant, A., Henne, S., Kristiansen, N. I., Minikin, A., Schumann, U., Seibert, P., Stebel, K., Thomas, H. E., Thorsteinsson, T., Tørseth, K., and Weinzierl, B.: Determination of time- and height-resolved volcanic ash emissions and their use for quantitative ash dispersion modeling: the 2010 Eyjafjallajökull eruption, Atmos. Chem. Phys., 11, 4333–4351, doi:10.5194/acp-11-4333-2011, 2011.
Swanson, S. E. and Beget, J.: Melting properties of volcanic ash, in: Volcanic Ash and Aviation Safety – Proceedings of the First International Symposium on Volcanic Ash and Aviation Safety, US Geological Survey Bulletin 2047, Seattle, Washington, USA, 1991.
Thomas, W., Erbertseder, T., Ruppert, T., van Roozendael, M., Verdebout, J., Meleti, C., Balis, D., and Zerefos, C.: On the retrieval of Volcanic Sulfur Dioxide Emissions from GOME backscatter measurements, J. Atmos. Chem., 50, 295–320, 2005.
Torres, O., Bhartia, P. K., Herman, J. R., Ahmad, Z., and Gleason, J.: Derivation of aerosol properties from satellite measurements of backscattered ultraviolet radiation. Theoretical basis, J. Geophys. Res., 103, 17099–17110, 1998.
van Geffen, J., van Roozendael, M., Di Nicolantonio, W., Tampellini, L., Valks, P., Erbertseder, T., and van der A, R.: Monitoring of volcanic activity from satellites as part of the GMES Service

AMTD
5, 4249–4283, 2012

Element Atmosphere (PROMOTE), Proceedings of the ENVISAT Symposium, 23–27 April 2007, Montreux, Switzerland, ESA publication SP-636, 2007.
Volz, F. E.: Infrared optical constants of ammonium sulphate, Sahara dust, volcanic pumice, and flyash, Appl. Optics, 12 564–568, 1973.
Warren, S. G.: Optical constants of ice from the ultraviolet to the microwave, Appl. Optics, 23, 1206–1225, 1984.
Wen, S. and Rose, W. I.: Retrieval of sizes and total masses of particles in volcanic clouds using AVHRR channels 4 and 5, J. Geophys. Res., 99, 5421–5431, 1994.
Zehner, C. (Ed.): Monitoring Volcanic Ash from Space, ESA-EUMETSAT Workshop on the 14 April to 23 May 2010 eruption at the Eyjafjöll volcano, South Iceland, ESA/ESRIN, STM-280, 2010.

AMTD
5, 4249–4283, 2012

Table 1. Mineral components used in the retrieval and source of optical constants.

Mineral	Obsidian	Palagonite	Bytownite (Plagioclase)	Orthoclase	Saponite	Forsterite (Olivine)	Augite (Clino-pyroxene)	Ortho-pyroxene
Source	Koike (1989)	Roush (1991)	Aronson (1979)	Aronson (1986)	Roush (1973)	Servoin and Pirou (1973)	Aronson (1979)	Roush (1991)

AMTD
5, 4249–4283, 2012

Table 2. Sensitivity of the number of IASI observations to aerosol optical depth thresholds (AOD) and maximum retrieval uncertainty (ERR) for the eruptive period from 5 June to 14 June 2011. For the analysis the threshold values for aerosol optical depth vary between 0.1 and 0.3 and the retrieval uncertainty between threshold values ranging from 30 % to 50 %.

AOD ERR Date	>0.1 <50 % n_{obs}	>0.1 <40 %	>0.1 <30 %	>0.2 <50 %	>0.2 <40 %	>0.2 <30 %	>0.3 <50 %	>0.3 <40 %	>0.3 <30 %
5 Jun	161	145	97	127	123	90	103	101	84
6 Jun	998	801	464	717	641	402	500	471	326
7 Jun	1089	942	630	729	667	456	460	449	309
8 Jun	1149	982	665	691	617	437	399	380	284
9 Jun	762	605	365	297	261	185	118	112	90
10 Jun	628	572	387	200	197	176	50	50	47
11 Jun	167	146	101	18	18	17	0	0	0
12 Jun	240	211	136	50	49	43	18	18	16
13 Jun	333	302	196	72	69	64	5	5	5
14 Jun	132	119	82	13	13	4	1	1	0
Total No. Obs	5659	4825	3123	2914	2655	1874	1654	1587	1161

AMTD
5, 4249–4283, 2012

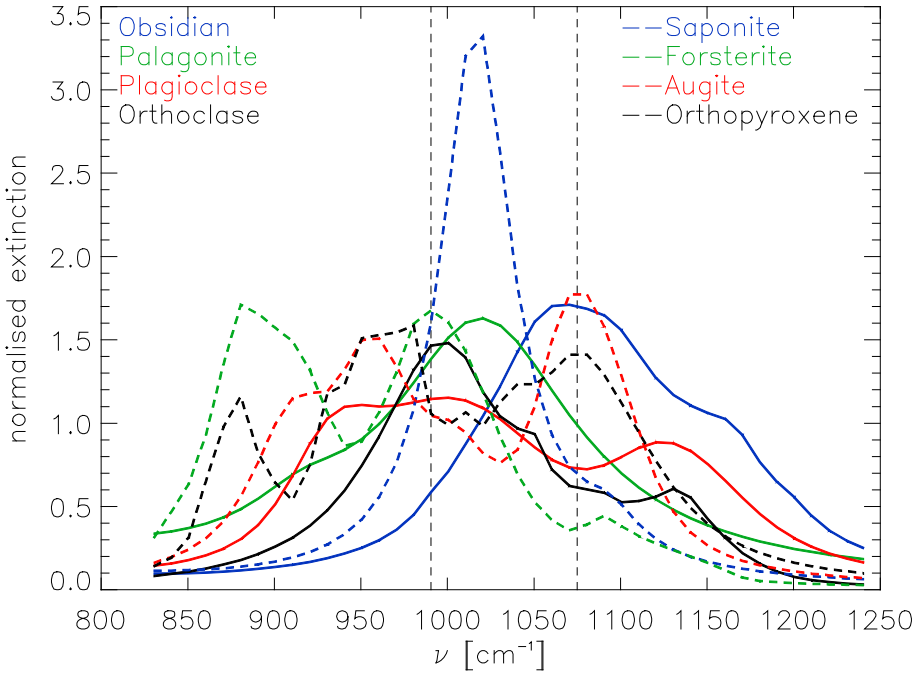

Fig. 1. Extinction spectra of volcanic minerals in wavenumber (ν) space. The vertical dashed black lines delimit the ozone absorption band not used by the retrieval (see Klüser et al., 2011).

AMTD
5, 4249–4283, 2012

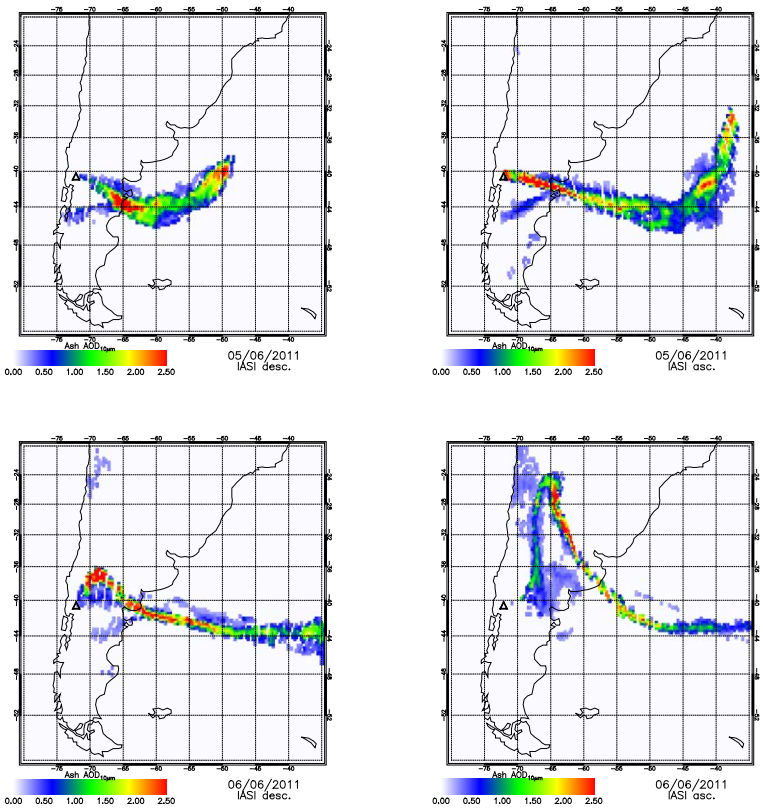

Fig. 2. Ash optical depth at 10 µm of the PCCE plume for 5 through 6 June. Descending (desc.) orbits represent morning observations, ascending (asc.) orbits are from local evening. The black triangle indicates the position of the volcano.

AMTD
5, 4249–4283, 2012

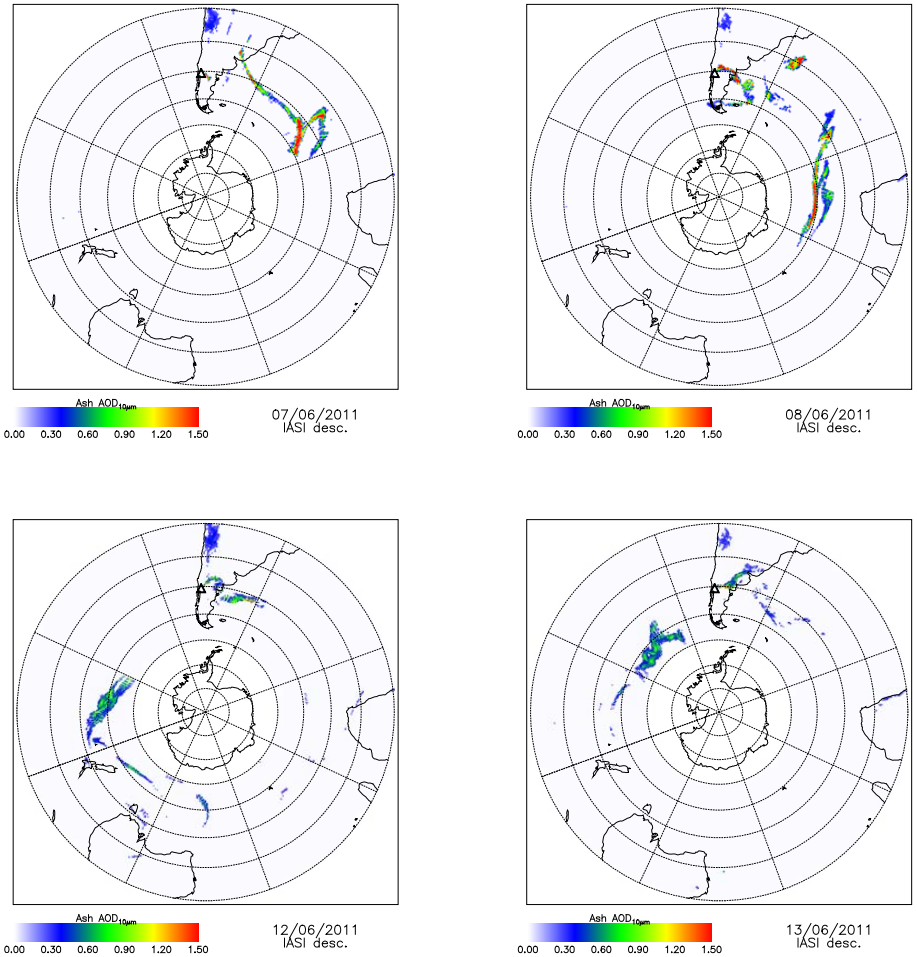

Fig. 3. The PCCE ash plume on its way around the Southern Hemisphere for descending MetOp orbits from 7, 8, 12 and 13 June.

AMTD
5, 4249–4283, 2012

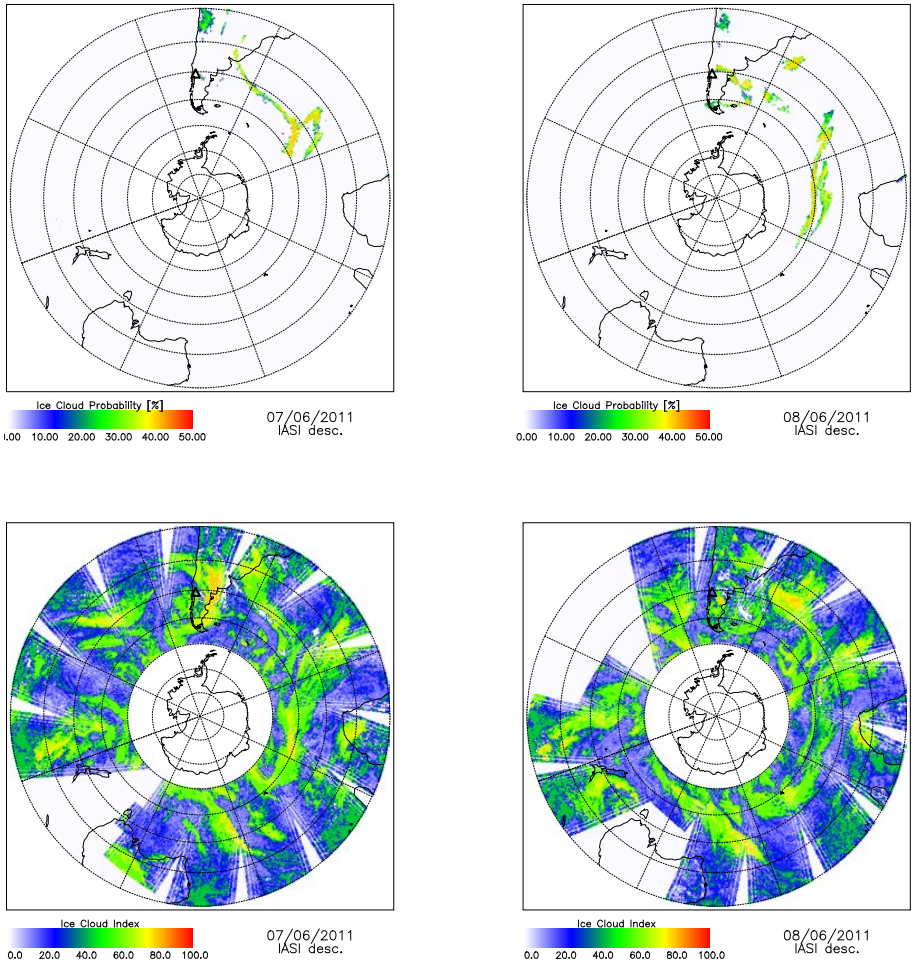

Fig. 4. Probability of ice crystals in ash plume for descending orbits of 7 and 8 June 2011 (top row) and ice cloud index for all IASI observations (bottom row).

AMTD
5, 4249–4283, 2012

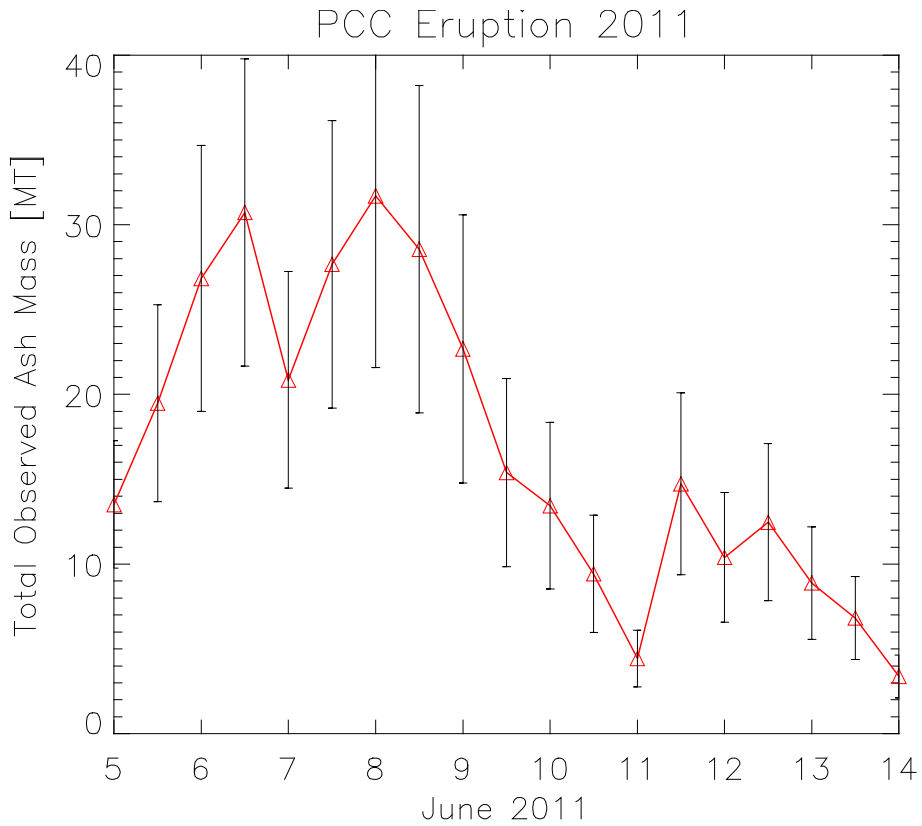

Fig. 5. Time series of the total PCCE ash plume mass as observed by IASI.

AMTD
5, 4249–4283, 2012

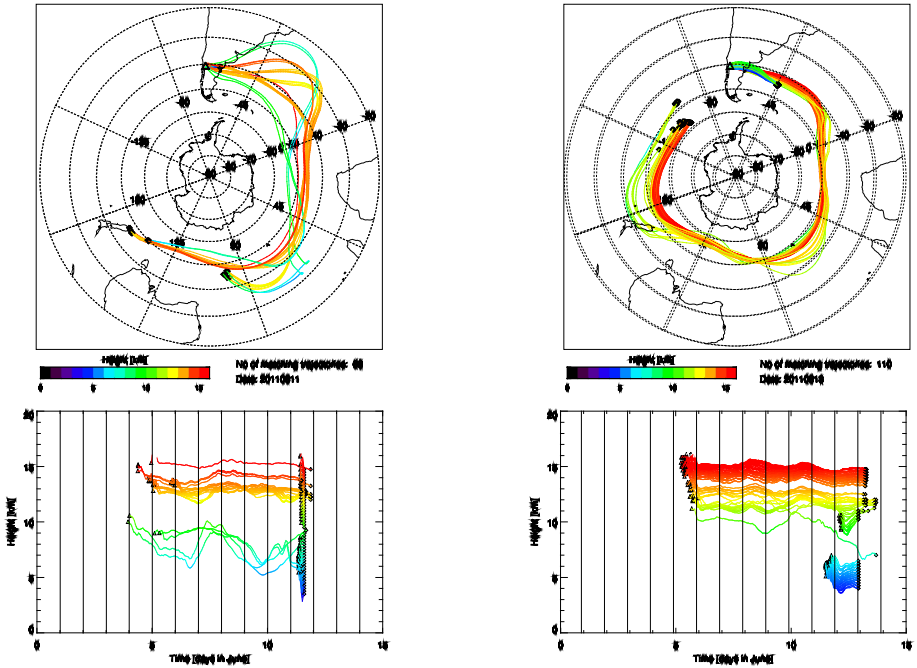

Fig. 6. Backward trajectories released for the IASI observations on 11 June (left) and 13 June (right) filtered for PCCE depicting the source-receptor relationship. In the bottom panel the matching backward trajectories are plotted as a function of height. The triangle symbolizes the volcano (source), the cross the observation (receptor where the backward trajectory was initialized). The observation time follows two groups, the ascending and descending orbit.

AMTD
5, 4249–4283, 2012

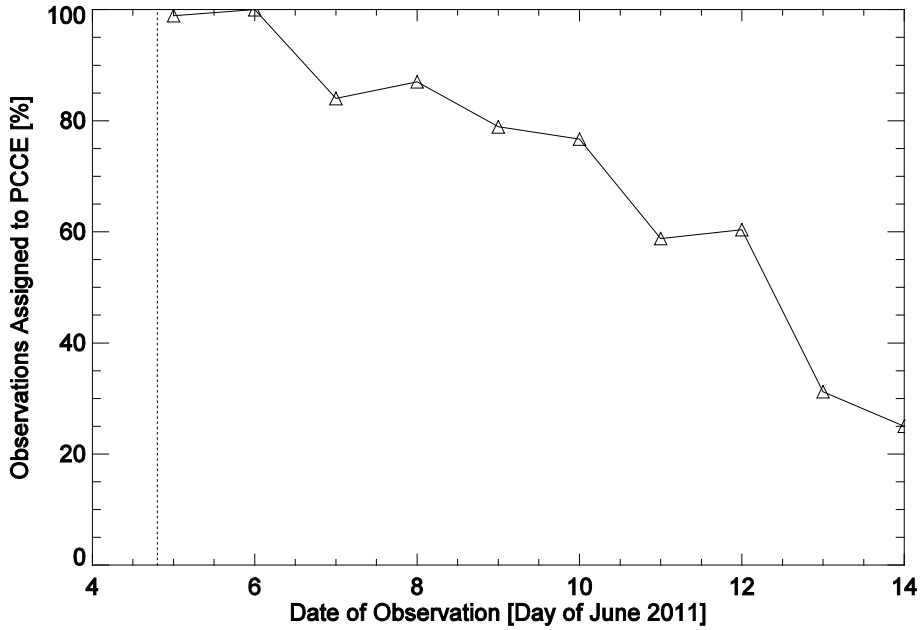

Fig. 7. Percentage of IASI observations per day that could be assigned to the PCCE source. The given dates refer to the date of observation. The dotted line indicates the onset of the eruption on 4 June 2011 at 19:15 UTC.

AMTD
5, 4249–4283, 2012

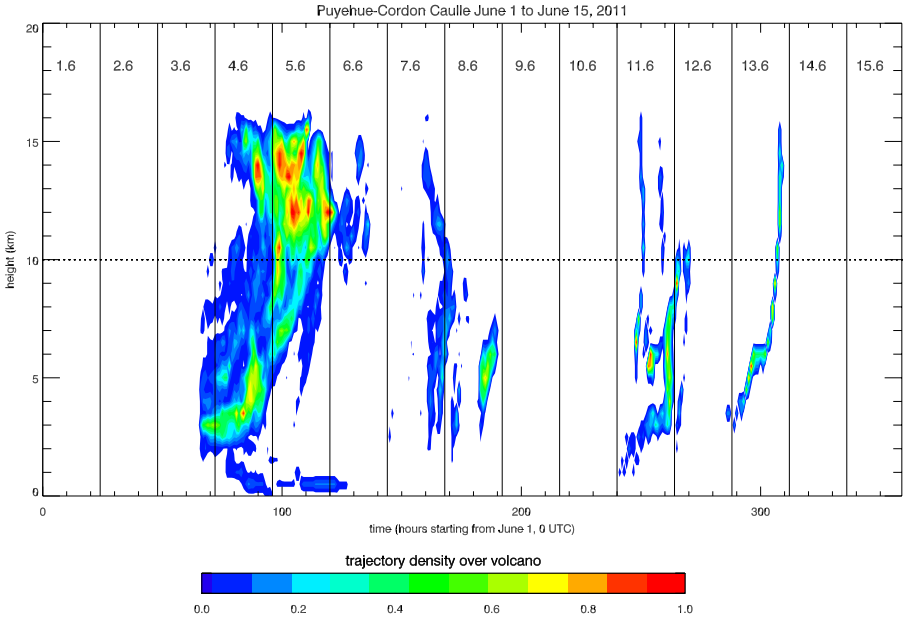

Fig. 8. Normalized trajectory density above PCC from 1 June to 15 June as indicator for the effective emission height of the volcanic ash derived by applying a source-receptor analysis using ensembles of backward trajectories.

AMTD
5, 4249–4283, 2012

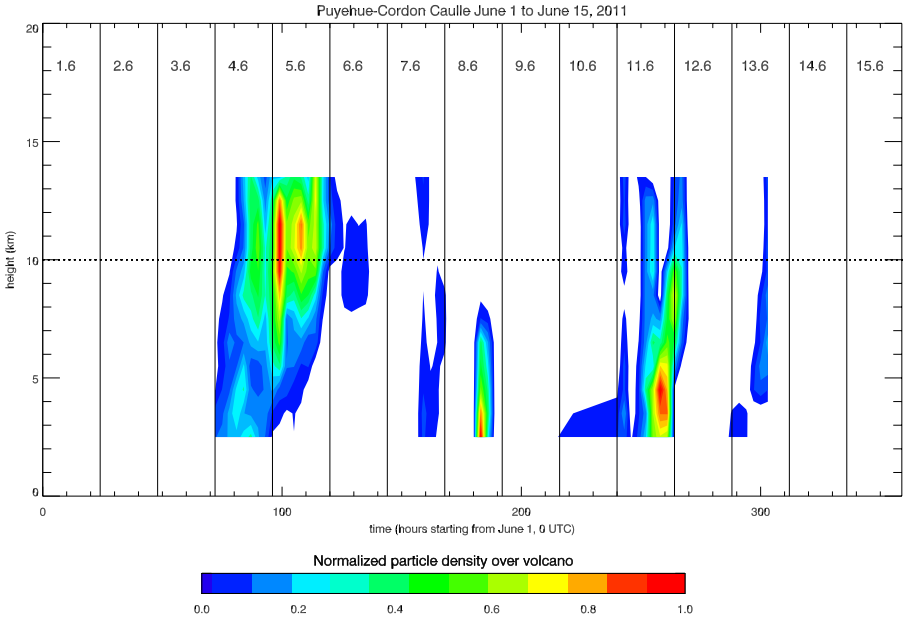

Fig. 9. Normalized particle density above PCC from 1 June to 15 June as indicator for the effective emission height of the volcanic ash derived by matching emitted particles with IASI observations.

AMTD
5, 4249–4283, 2012